Original Article

Bone Marrow Mononuclear Cells Restore Normal Mitochondrial Ca^{2+} Handling and Ca^{2+}-Induced Depolarization of the Internal Mitochondrial Membrane by Inhibiting the Permeability Transition Pore After Ischemia/Reperfusion

Clara Rodrigues-Ferreira[1,2], Jarlene Alécia Lopes[1,3], Priscila Fonseca Carneiro[1], Cristiane dos Santos Lessa[4], Antonio Galina[4], and Adalberto Vieyra[1,3,5,6] (iD)

Abstract

Acute kidney injury due to ischemia followed by reperfusion (IR) is a severe clinical condition with high death rates. IR affects the proximal tubule segments due to their predominantly oxidative metabolism and profoundly altered mitochondrial functions. We previously described the impact of IR on oxygen consumption, the generation of membrane potential ($\Delta\Psi$), and formation of reactive oxygen species, together with inflammatory and structural alterations. We also demonstrated the benefits of bone marrow mononuclear cells (BMMC) administration in these alterations. The objective of the present study has been to investigate the effect of IR and the influence of BMMC on the mechanisms of Ca^{2+} handling in mitochondria of the proximal tubule cells. IR inhibited the rapid accumulation of Ca^{2+} (Ca^{2+} green fluorescence assays) and induced the opening of the cyclosporine A-sensitive permeability transition pore (PTP), alterations prevented by BMMC. IR accelerated Ca^{2+}-induced decrease of $\Delta\Psi$ (Safranin O fluorescence assays), as evidenced by decreased requirement for Ca^{2+} load and $t_{1/2}$ for complete depolarization. Addition of BMMC and ADP recovered the normal depolarization profile, suggesting that stabilization of the adenine nucleotide translocase (ANT) in a conformation that inhibits PTP opening offers a partial defense mechanism against IR injury. Moreover, as ANT forms a complex with the voltage-dependent anion channel (VDAC) in the outer mitochondrial membrane, it is possible that this complex is also a target for IR injury—thus favoring Ca^{2+} release, as well as the supramolecular structure that BMMC protects. These beneficial effects are accompanied by a stimulus of the citric acid cycle—which feed the mitochondrial complexes with the electrons removed from different substrates—as the result of accentuated stimulus of citrate synthase activity by BMMC.

Keywords

renal ischemia/reperfusion, bone marrow mononuclear cells, mitochondrial Ca^{2+} handling, permeability transition pore, mitochondrial membrane potential

[1] Carlos Chagas Filho Institute of Biophysics, Federal University of Rio de Janeiro, Rio de Janeiro, Brazil
[2] Roberto Alcântara Gomes Institute of Biology, Rio de Janeiro State University, Rio de Janeiro, Brazil
[3] National Center for Structural Biology and Bioimaging, Federal University of Rio de Janeiro, Rio de Janeiro, Brazil
[4] Leopoldo de Meis Institute of Biochemistry, Federal University of Rio de Janeiro, Rio de Janeiro, Brazil
[5] National Institute of Science and Technology for Regenerative Medicine, Federal University of Rio de Janeiro, Rio de Janeiro, Brazil
[6] Graduate Program of Translational Biomedicine, Grande Rio University, Duque de Caxias, Brazil

Corresponding Author:
Adalberto Vieyra, Carlos Chagas Filho Institute of Biophysics, Federal University of Rio de Janeiro, Rio de Janeiro 21941-590, Brazil.
Email: avieyra@biof.ufrj.br

Introduction

Renal ischemia followed by reperfusion (IR) is characterized by an initial restriction of renal blood flow, followed by restoration of circulation and O_2 supply[1,2]. The sequence of IR events is very common in acute kidney injury (AKI), one of the most severe clinical conditions in intensive care units worldwide[3]. Death from AKI is very frequent; more than 1.7 million of deaths per year are caused by AKI, with 1.4 million in low- and middle-income countries[4]. Survivors frequently develop chronic kidney disease (CKD)[5], a risk factor for AKI[6].

Renal proximal tubule cells are particularly vulnerable to IR because of their intense oxidative metabolism, mitochondria from these cells being particularly sensitive to IR injury[7]. In the absence of O_2, depletion of ATP rapidly occurs, leading to cell death with a concomitant and a sudden decrease in the glomerular filtration rate and deregulation of the renal hemodynamics as a whole[8]. During reoxygenation, an important burst of reactive oxygen species (ROS) occurs as a result of an uncontrolled premature transference of electrons to O_2 to form $O_2^{\bullet-}$ in steps before physiological transfer at the level of cytochrome oxidase[9,10]. A high production of ROS is also the result of Ca^{2+} release from the intra-mitochondrial compartment, followed by activation of mitochondrial Ca^{2+}-dependent cytosolic proteases, the xanthine oxidase pathway, and NADPH oxidases, though the latter are considered secondary to the initial mitochondrial burst of mitochondrial $O_2^{\bullet-}$[11].

The central role of uncontrolled Ca^{2+} handling in the opening of the permeability transition pore (PTP) during IR, in the collapse of mitochondrial membrane potential ($\Delta\Psi$) and in oxidant damage, is widely accepted[12,13]. However, the molecular mechanisms by which IR alters mitochondrial Ca^{2+} homeostasis and the Ca^{2+}-induced alterations of $\Delta\Psi$, in an environment of exacerbated production of $O_2^{\bullet-}$ and other ROS, are not fully understood. Answers to questions are far from clear: What are the mechanisms by which cell therapies—a promise that emerged over the two last decades in the prevention and regeneration of renal lesions[14–18]—could be beneficial in preventing or repairing mitochondrial damage in IR? Are these potential mechanisms associated with preservation of mitochondrial Ca^{2+} transport mechanisms and physiological Ca^{2+}-induced modulation of $\Delta\Psi$?

We previously described the influence of renal IR on electron fluxes, generation of the $\Delta\Psi$, ATP synthesis, ROS generation, *S*-nitrosylation of proteins in renal cells, apoptosis, and inflammatory responses. We also investigated the effects of bone marrow mononuclear cells (BMMC) in these processes, correlated to the recovery of tubular lesions[19]. The beneficial properties of BMMC, which have been centrally used in renal regenerative medicine for a number of years[15,20–22], remerged as promising again since the discovery of the potential therapeutic role of extracellular vesicles (EVs) secreted[23,24] by the most abundant parcel of their cell population, CD11^{+} CD29^{−} granulocytes from the CD45^{+} cluster[19].

The object of the present study has been to investigate how renal IR modifies Ca^{2+} transport mechanisms in renal mitochondria in rats, together with the Ca^{2+}-induced depolarization of the internal mitochondrial membrane, and to see whether BMMC can recover—or prevent—the possible functional alterations provoked by acute IR. Participation of the Ca^{2+}-provoked opening of PTP—with the possible beneficial influence of BMMC—has been investigated. As the electrons removed from the substrates oxidized in the citric acid cycle feed the mitochondrial transport system, we also investigated the impact of IR and the effects of BMMC on the citrate synthase activity. We chose this enzyme because it catalyzes the supply of 2C fragments from acetyl-CoA (AcCoA) at the first step of the cycle[25].

Materials and Methods

Animals

Adult male Wistar rats (180–200 g) obtained from the vivarium of the Leopoldo de Meis Institute of Biochemistry at Federal University of Rio de Janeiro and Oswaldo Cruz Institute (Rio de Janeiro) were housed at 22°C in ventilated cages under humidity control and 12 h:12 h light/dark cycle, receiving commercial chow (Purina Agribands, Paulínia, Brazil) and filtered water *ad libitum*. The experimental protocols followed the guidelines of the local Committee of Ethics in the Use of Animals for Research (approval number: 104).

After 1 week of acclimatization, the animals were divided into three groups: (i) SHAM with opening of the abdominal cavity and smooth manipulation of the renal pedicles, (ii) IR: bilateral clamping of the renal arteries with silver clamps for 30 min followed by 1 h of reperfusion (one specific experiment was carried out after 24 h of reperfusion), and (iii) IR rats that received subcapsularly 1×10^6 bone marrow–derived mononuclear cells (IR + BMMC) 1 h before arterial clamping. Before surgery the animals were anesthetized by intraperitoneal injection of 0.4 ml of a solution containing 5% w/v ketamine hydrochloride (Cristália, Itapira, Brazil) and 0.02 mg/ml xylazine hydrochloride (Bayer SA, São Paulo, Brazil) (proportion 3:1). The rats in the groups given 24 h reperfusion were sutured with cotton thread 3.0, locally treated with lidocaine to suppress pain, and returned to individual cages. All animals were killed by decapitation.

Cells

The source of cells was bone marrow, which was obtained by flushing the femurs and tibias with saline of rats of the same gender and age, and with similar body mass to those used to compose the three experimental groups given above. Isolation of BMMC was carried out by using Histopaque®
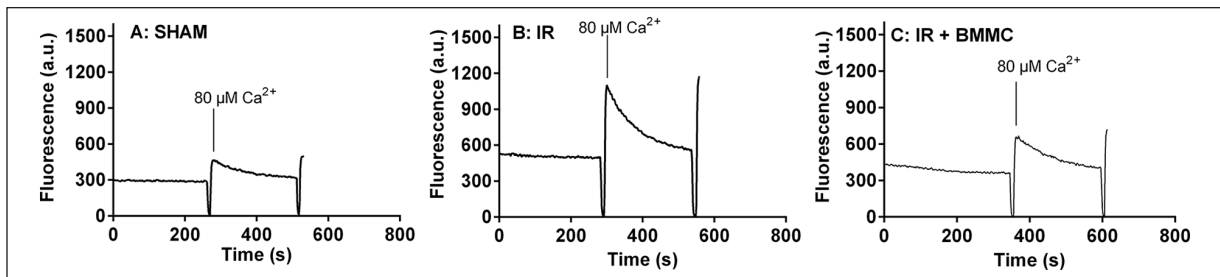
Figure 1. Rapid mitochondrial Ca^{2+} uptake is inhibited by IR and totally recovered by BMMC treatment. Representative recordings of Ca^{2+} green fluorescence (extra-mitochondrial Ca^{2+}) after a single pulse of 80 μM $CaCl_2$ (160 nmol Ca^{2+} in a 2 ml cuvette) to mitochondria suspended in MIR05 (0.5 mg/ml) and energized with 10 mM succinate in the presence of 100 μM ADP. Mitochondria from SHAM (A), IR (B), and IR + BMMC (C) were isolated and assayed after 1 h of reperfusion. In the case of the SHAM rats, which had only gentle manipulation of the vascular renal pedicle, the time of "reperfusion" refers to a time that was the same as for the IR and IR + BMMC animals after release from clamping. IR: ischemia followed by reperfusion; BMMC: bone marrow mononuclear cells.

(Sigma-Aldrich, Saint Louis, MO, USA). Bone marrow samples were initially centrifuged for 10 min at 395 × *g* (25°C) and the recovered sediment resuspended in 3.5 ml DMEM without serum, homogenized, layered on to 3.5 ml Histopaque®, and centrifuged at 403 × *g* for 30 min (initial acceleration and final deceleration lasting 120 and 150 s to preserve the gradient). The cells localized in the interface between DMEM and Histopaque® were carefully removed, suspended in DMEM, recentrifuged at 395 × *g*, suspended again in DMEM, and used within 2 h. Viability was assessed with trypan blue. The immunophenotype of the cells was characterized as described in the previous studies[19,23,24,26]. Their viability was also assessed with trypan blue. Four subpopulations were characterized from the cluster of differentiation 45 ($CD45^+$) cell population (95% of total cells): (i) T helper lymphocytes (0.15%), (ii) T cytotoxic lymphocytes (1.5%), (iii) monocytes (13%), and (iv) granulocytes (54%)[19]. For a fuller illustration of the phenotype characterization of the used BMMC, see, for example, Fig. 1 in Beiral et al.[19] Controls for tracing of BMMC in the cortical renal parenchyma were carried out with amine-reactive Cell Trace™ Far Red DDAO-succinimidyl ester (Invitrogen, Grand Island, NY, USA) to obtain three-dimensional (3D) reconstructions visualized in an ApoTome microscope (ApoTome Axio Imager M2, Carl Zeiss, Inc., Jena, Germany)[19].

Mitochondrial Isolation

Each pair of kidneys was rinsed with a cold solution containing 250 mM sucrose, 10 mM HEPES–Tris (final pH 7.4), 2 mM ethylenediaminetetraacetic acid (EDTA), and 0.15 mg/ml trypsin inhibitor (Sigma-Aldrich), which was used in all the following steps. The *cortex corticis*, part of renal tissue where >90% of the cell population corresponds to proximal tubules[27], was rinsed and then homogenized by hand through 11 cycles in a 30 ml glass homogenizer (Wheaton Sci., Wheaton, IL, USA). After centrifugation at 600 × *g* for 5 min to remove unbroken cells, nuclei, and cell debris, the

supernatant was centrifuged at 12,000 × *g* and the sediment washed twice in 10 ml of the above solution at the same speed, finally being suspended in 0.3 ml of the same solution containing 10 mg/ml bovine serum albumin (BSA; fatty acid-free; Sigma-Aldrich) and used immediately. Protein content was quantified by Folin phenol reagent[28].

Mitochondrial Ca^{2+} Accumulation and Release

Calcium uptake was measured by using a Calcium green 5N (Life Technologies, Carlsbad, CA, USA) probe and a Hitachi fluorometer model F-3010 (Hitachi Ltd., Tokyo, Japan) at 506 nm (excitation)/532 nm (emission). The assay medium (37°C) contained 0.5 mg/ml of mitochondria, MIR05 without EGTA (110 mM sucrose, 3 mM $MgCl_2$, 20 mM taurine, 60 mM MES, 20 mM HEPES, 10 mM KH_2PO_4, and 1 mg/ml BSA), pH adjusted to 7.1 by addition of KOH, and supplied with 100 μM ADP, 0.2 μM Calcium green, and 1 μM rotenone. Recordings in the presence or absence of 1 μM cyclosporine A (CsA) were initiated just before addition of 10 mM succinate and successive pulses of 80 μM $CaCl_2$ at 2-min intervals. After a fast increase of fluorescence that corresponded to Ca^{2+} binding to the extra-mitochondrial Calcium green, a decrease with two components occurred (see "Results" section): a very fast one—which cannot be resolved by this method—and a slower one. The rate of this component was measured by determination of the slope over 20 s from the fluorescence peak. After several additions, the uptake stopped and a sudden release occurred.

Ca^{2+}-Induced Depolarization of the Inner Mitochondrial Membrane

The Ca^{2+}-induced modifications of mitochondrial transmembrane potential (ΔΨ) were measured by the evolution of fluorescence of Safranin O (Sigma-Aldrich) at 495 nm (excitation)/586 nm (emission) in the presence of energized mitochondria. The mitochondria were preincubated for 2

min in the chamber of the Hitachi F-3010 fluorometer at 37°C with a solution containing 320 mM mannitol, 10 mM Tris HCl (pH 7.4), 8 mM Tris-phosphate (H_3PO_4 neutralized with Tris base up to pH 7.4), 4 mM $MgCl_2$, 1 mg/ml BSA fatty acid-free (Sigma-Aldrich), 1 μM rotenone (Sigma-Aldrich), and 5 μM Safranin O (Sigma-Aldrich), in the absence or presence of 1 mM ADP. After mitochondrial energization with 10 mM succinate and rapid decrease in fluorescence intensity, successive pulses of 10 μM $CaCl_2$ allowed measurements of total Ca^{2+} load ($[Ca^{2+}]_t$) required for complete depolarization (completed by adding 1 μM FCCP) and of the time necessary for 50% recovery of the baseline ($t_{1/2}$).

Citrate Synthase Activity

Total citrate synthase activity was measured by following the formation of 5-thio-2-nitrobenzoic acid (TNB) during the irreversible colorimetric reaction:

$$CoA\text{-}SH + DTNB \rightarrow TNB + CoA\text{-}S\text{-}S\text{-}TNB,$$

coupled *in vitro* to the reaction catalyzed by mitochondrial citrate synthase:

$$OAA + AcCoA \rightarrow Citrate,$$

where CoA-SH is coenzyme A, DTNB is 5,5′-dithiobis-(2-nitrobenzoic acid), OAA is oxaloacetate, and AcCoA is acetyl-CoA. The yellow product, TNB, was quantified by measuring absorbance (molar absorption coefficient 13.6 mM^{-1} cm^{-1}) at 412 nm in a spectrometer UV-1800 UV-VIS (Shimatzu, Kyoto, Japan). The assays (at 25°C) were carried out in 1 ml of medium containing 0.1 mg/ml total mitochondrial protein preincubated for 2 min in 10 mM Tris HCl (final pH 8.5), 10 mM KH_2PO_4, 2 mM EDTA, 0.1% (w/v) Triton X-100, 0.1 mM AcCoA (Sigma-Aldrich), and 2 mM DTNB (Sigma-Aldrich). The reaction was started by adding 10 mM OAA (Sigma-Aldrich) and recorded over 10 min.

Statistical Analysis

Bar graphs and symbols represent means ± SEM (standard error of the mean). One-way analysis of variance (ANOVA) followed by Tukey's test was used to assess differences among three mean values, and unpaired Student's *t* test was used for the comparison of two means, as detailed in the corresponding figure legends or in the text. Correlation between two variables was assessed by the least squares method. $P < 0.05$ was considered statistically significant; *P* values are given within the panels of Figs. 5, 7, and 8, and in the legend to Fig. 6. Calculations were carried out using GraphPad Prism®, Version 6 (GraphPad Software, Inc., San Diego, CA, USA).

Results

IR Decreased Rapid Ca^{2+} Uptake by Mitochondria From Proximal Tubule Cells: Total Recovery by BMMC

Fig. 1 shows representative recordings of the time course of Ca^{2+} green fluorescence after a single addition of 80 μM Ca^{2+} to suspensions of mitochondria isolated 1 h after the beginning of reperfusion, or the equivalent time in SHAM rats. The traces show a very fast increase in Ca^{2+} green fluorescence followed by a slower decrease. This profile corresponds to the signal triggered by Ca^{2+} addition, followed by the entrance of the cation into the mitochondrial matrix. The height of the peak is lower in mitochondria from SHAM rats (Fig. 1A) than in mitochondria isolated from proximal tubules of rats submitted to IR (Fig. 1B), indicating that more Ca^{2+} remained transiently in the medium in this group. This means that a rapid mitochondrial Ca^{2+} uptake, which occurs in time intervals that cannot be resolved with this approach, became impaired as the result of the IR lesions. The time course of Ca^{2+} green fluorescence in IR rats that received subcapsular administration of BMMC 1 h before bilateral arterial clamping (IR + BMMC group) was similar to that in SHAM rats (Fig. 1C).

The differences in the evolution of Ca^{2+} green fluorescence are better perceived after successive Ca^{2+} pulses and quantification of the percent departure of fluorescence from the baseline 2 min after each addition. Increasing departure indicates that more Ca^{2+} remains in the medium after each uptake cycle. Fig. 2 shows representative recordings in the absence (A–C) and presence of 1 μM CsA (D–F). There is a progressive exponential increase of extra-mitochondrial Ca^{2+}, which is more accentuated in the case of IR rats, and was recovered in the group receiving BMMC [compare circles in Fig. 2H with those in Fig. 2G (SHAM) and Fig. 2I (IR + BMMC)]. The values of percent departure from baseline were lower when CsA was present in the assay medium and more Ca^{2+} could be added before the sudden efflux, as demonstrated by the shift of the triangle symbols to 720 μM Ca^{2+} (compare with the corresponding circles at 560 μM Ca^{2+}).

The rate constant, *k*, obtained with the use of the exponential function, $y = y_o e^{kx}$, allows quantitative comparison of the velocity by which ΔF (ie, extra-mitochondrial Ca^{2+}) increases per minute after each Ca^{2+} addition. In the absence of CsA (circles), their values were 0.0032, 0.0051, and 0.0043 $μM^{-1}$ min^{-1} for SHAM, IR, and IR + BMMC rats, respectively, indicating that 50% less Ca^{2+} were transported inside the renal mitochondria from IR rats and that a significant return toward SHAM rates occurred in the group receiving BMMC. Differences among the three experimental groups also emerged from a comparison of the ΔF at 560 μM Ca^{2+}: $P < 0.0001$ (SHAM vs IR), $P = 0.0244$ (SHAM vs IR + BMMC), and $P = 0.0009$ (IR vs IR + BMMC). The changes provoked
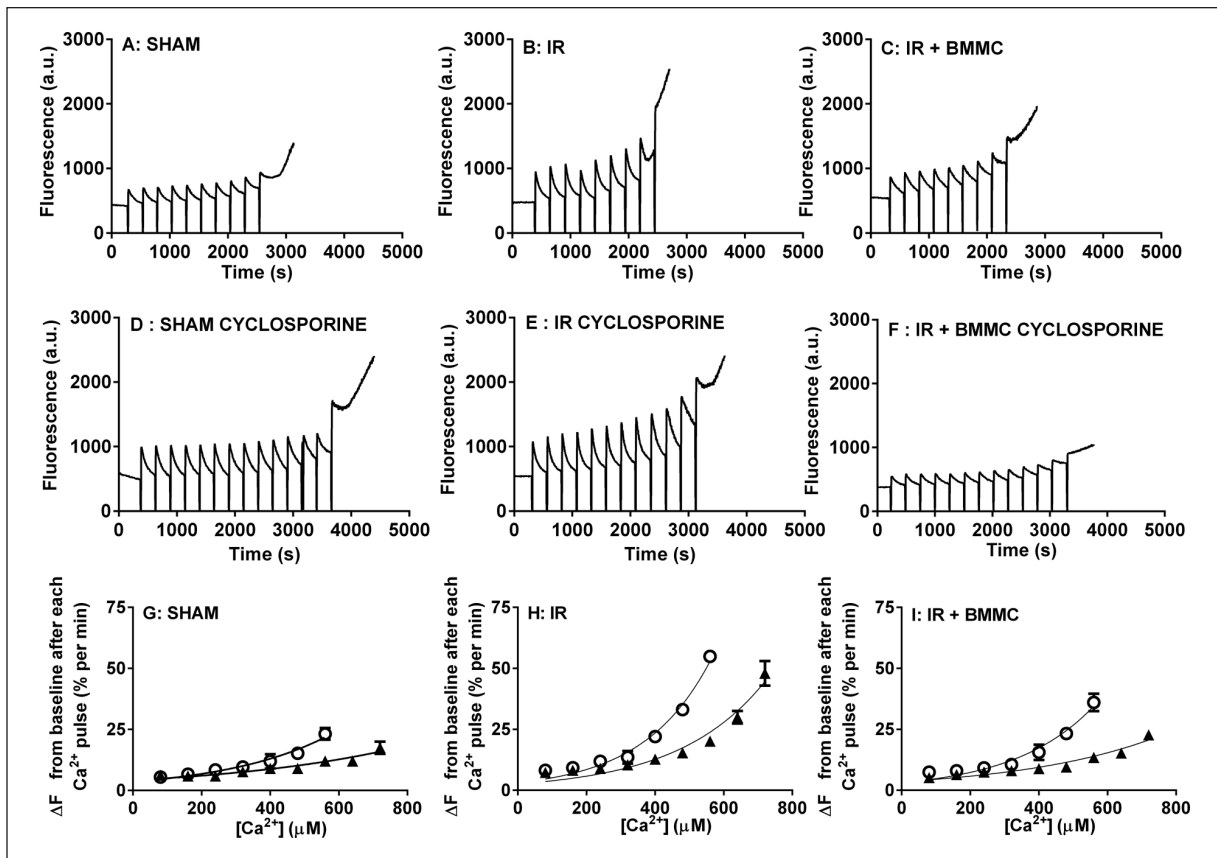
Figure 2. Time course of mitochondrial Ca^{2+} accumulation after successive additions of Ca^{2+}: effect of CsA. (A–C) Representative traces showing the evolution of Ca^{2+} green fluorescence after successive Ca^{2+} pulses in the absence of CsA. (D, E) Representative traces showing the evolution of Ca^{2+} green fluorescence after successive Ca^{2+} pulses in the presence of 1 μM CsA. Mitochondria (0.5 mg/ml) from SHAM (A, D), IR (B, E), or IR + BMMC (C, F) were incubated in Ca^{2+} green-containing media (MIR05) plus 100 μM ADP and energized with 10 mM succinate. The samples were successively supplied with CaCl$_2$ pulses (80 μM) at 2-min intervals. The final ascending part of the traces represents the sudden Ca^{2+} efflux from the intra-mitochondrial compartment. (G–I) Percent change of Ca^{2+} green fluorescence (departure from baseline) 2 min after each addition of CaCl$_2$ to give the Ca^{2+} concentrations shown on the *abscissae*, in the absence (circles) or presence (triangles) of 1 μM CsA. In some cases, the error bar is smaller than the symbol size. The smooth lines were adjusted to the experimental points (means ± SEM) by using the function $y = y_o e^{kx}$, where y corresponds to the percent increase of fluorescence from baseline per minute after each Ca^{2+} addition, y_o corresponds to the theoretical departure of fluorescence before the first Ca^{2+} addition, k is the constant of fluorescence increase (ie, the constant of extra-mitochondrial Ca^{2+} increase after each Ca^{2+} pulse), x is the cumulative Ca^{2+} concentration, and e has the usual meaning. Using one-way ANOVA followed by Tukey's test, we compared the means ($n = 5{-}7$ different mitochondrial preparations) of fluorescence changes at 560 μM Ca^{2+} in the absence of CsA. The P values are given in the text. In the presence of CsA, the means of fluorescence changes ($n = 5{-}8$) were compared at 720 μM Ca^{2+}, the P values also being given in the text. CsA: cyclosporine A; IR: ischemia followed by reperfusion; BMMC: bone marrow mononuclear cells; SEM: standard error of the mean; ANOVA: analysis of variance.

by CsA (triangles) are twofold. First, the rate constant k decreased in all groups; their values dropped to 0.0019 (SHAM), 0.0039 (IR), and 0.0024 μM^{-1} min^{-1} (IR + BMMC). Second, the difference in ΔF per minute at 720 μM Ca^{2+} between SHAM and IR + BMMC disappeared ($P >$ 0.6437), that is, CsA contributed to the entire recovery of Ca^{2+} influx induced by BMMC in the absence of the drug. The values for the other comparisons were $P = 0.0001$ (SHAM vs IR) and $P = 0.0003$ (IR vs IR + BMMC).

The first-order and CsA-sensitive decrease in rapid Ca^{2+} entry into the renal intra-mitochondrial compartment in IR rats, as demonstrated by the greater height of the green

fluorescence peak and the greater k value, was accompanied by modifications in two processes: one was related to the slower phase of Ca^{2+} uptake, and the other was related to the capacity of Ca^{2+} retention. Fig. 3A shows that the decrease in Ca^{2+} green fluorescence, which corresponds to the slow Ca^{2+} entry, was faster in mitochondria from IR rats (circles) than SHAM (squares) or IR + BMMC rats (triangles). This observation is additional evidence that less Ca^{2+} entered the mitochondria through the faster component and that intra-mitochondrial concentration was initially lower at the beginning of the slower uptake phase. Moreover, the tendency of Ca^{2+} efflux in IR mitochondria gradually rose from the
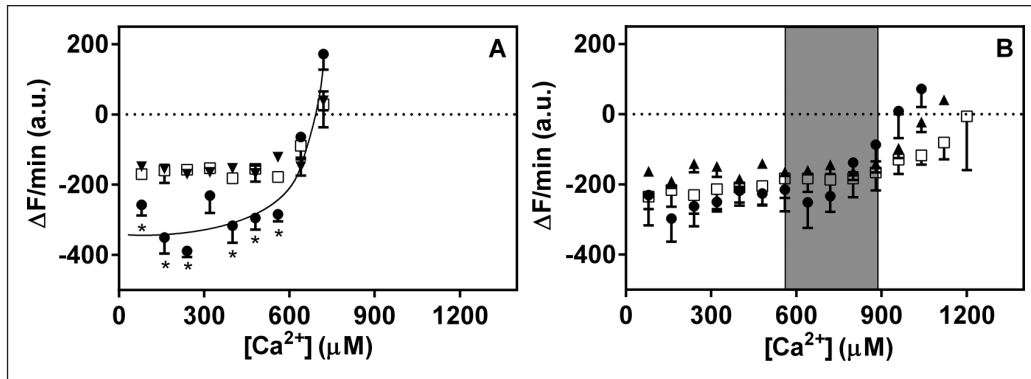
Figure 3. Rate of Ca^{2+} green fluorescence decay (ΔF/min) from the peaks obtained after each pulse of 80 µM CaCl$_2$ at 2-min intervals in media containing mitochondria (0.5 mg/ml), energized with 10 mM succinate and supplied with 100 µM ADP in the absence (A) or in the presence of 1 µM CsA (B). The rates were measured during the linear phase of decay (20 s) after each CaCl$_2$ pulse. The *abscissae* show the accumulated Ca^{2+} in the medium. The symbols correspond to SHAM (squares), IR (circles), and IR + BMMC rats (triangles). The dotted horizontal line at ΔF/min = 0 indicates Ca^{2+} influx = Ca^{2+} efflux, and negative values indicate that Ca^{2+} influx > Ca^{2+} efflux. Values are means ± SEM. In some cases, the error bars are smaller than the symbol size. The smooth continuous curve in (A) (circles), drawn by hand, reveals an initially very slow and then a sudden tendency to Ca^{2+} efflux. The shaded area in (B) indicates the extra [Ca^{2+}] that can be provided to the medium containing IR mitochondria, when CsA is present, before the pulse that triggers the rapid Ca^{2+} efflux. In (A), points represent means of 4 (SHAM), 5 (IR), and 4 (IR + BMMC) determinations carried out by using different mitochondrial preparations. In (B), points represent means of 4 (SHAM), 6 (IR), and 4 (IR + BMMC) determinations, also carried out with the use of different mitochondrial preparations. In (A), asterisks indicate statistically different IR values with respect to SHAM and IR + BMMC (one-way ANOVA followed by Tukey's test comparing Ca^{2+} concentration-matched values). No differences were found between SHAM and IR + BMMC across the range of Ca^{2+} concentrations. In (B), no differences were found among the three groups across the range of Ca^{2+} concentrations. CsA: cyclosporine A; IR: ischemia followed by reperfusion; BMMC: bone marrow mononuclear cells; SEM: standard error of the mean; ANOVA: analysis of variance.

beginning of the additions of Ca^{2+} (smooth curve in Fig. 3A). In the assays carried out in the presence of 1 µM CsA (Fig. 3B), the rates of slow Ca^{2+} entry were similar in the three groups and additional Ca^{2+} loads—which totaled 320 µM (55% more) in IR mitochondria—could be added before any tendency of efflux was established (see the shaded area in Fig. 3B).

IR Alters the Response to Ca^{2+} of Mitochondrial Membrane Potential: Effect of BMMC and ADP

IR-induced alteration in mitochondrial Ca^{2+} handling also had an impact on the Ca^{2+} response of the membrane potential of energized mitochondria (Figs. 4 and 5). The representative recordings of Safranin O fluorescence after Ca^{2+} addition were investigated in the absence (Fig. 4A–C) and in the presence of 1 mM ADP (Fig. 4D–F). After mitochondrial energization by addition of succinate (arrows), successive pulses of 10 µM Ca^{2+} provoked a progressive depolarization of the inner mitochondrial membrane, which was faster in mitochondria isolated from kidneys submitted to with IR than in the SHAM and IR + BMMC groups (compare Fig. 4B with Fig. 4A, C). As in the case of Ca^{2+} handling measurements (Figs. 2 and 3), administration of BMMC before the IR episode partially restored the depolarization profile to that of the SHAM group. Ca^{2+}-induced depolarization was slower in the presence of ADP (Fig.

4D–F); however, it remained accelerated in IR mitochondria (compare Fig. 4E with Fig. 4D, F).

Quantification of the total Ca^{2+} load required for the return to baseline of fluorescence ([Ca^{2+}]$_t$) and the time required for half-depolarization ($t_{1/2}$) is presented in Fig. 5. In IR mitochondria, 40% less [Ca^{2+}]$_t$ sufficed for total depolarization (Fig. 5A), which also took place with a $t_{1/2}$ that is 45% lower (Fig. 5B). Administration of BMMC totally normalized [Ca^{2+}]$_t$, with a partial effect on $t_{1/2}$ (Fig. 5A, B). When assayed in the presence of ADP, [Ca^{2+}]$_t$ was similar in the three groups (Fig. 5C), with ADP-induced increases of 70%, 150%, and 70% in SHAM, IR, and IR + BMMC, respectively, compared with the values in the absence of the nucleotide (Fig. 5C vs A). The same profile was found for $t_{1/2}$, which also increased 60%, 160%, and 80% when one compares the same experimental group in the presence and absence of ADP (Fig. 5D vs B). Despite the small differences in the responses of [Ca^{2+}]$_t$ and $t_{1/2}$ to BMMC and ADP, the two parameters are closely associated in all conditions (Fig. 6): A single function was adjusted to the ensemble of different experimental points ($P < 0.0001$).

Stimulation of Citrate Synthase Activity by BMMC

The negative impact of IR in renal mitochondrial respiration and its recovery by BMMC has previously been
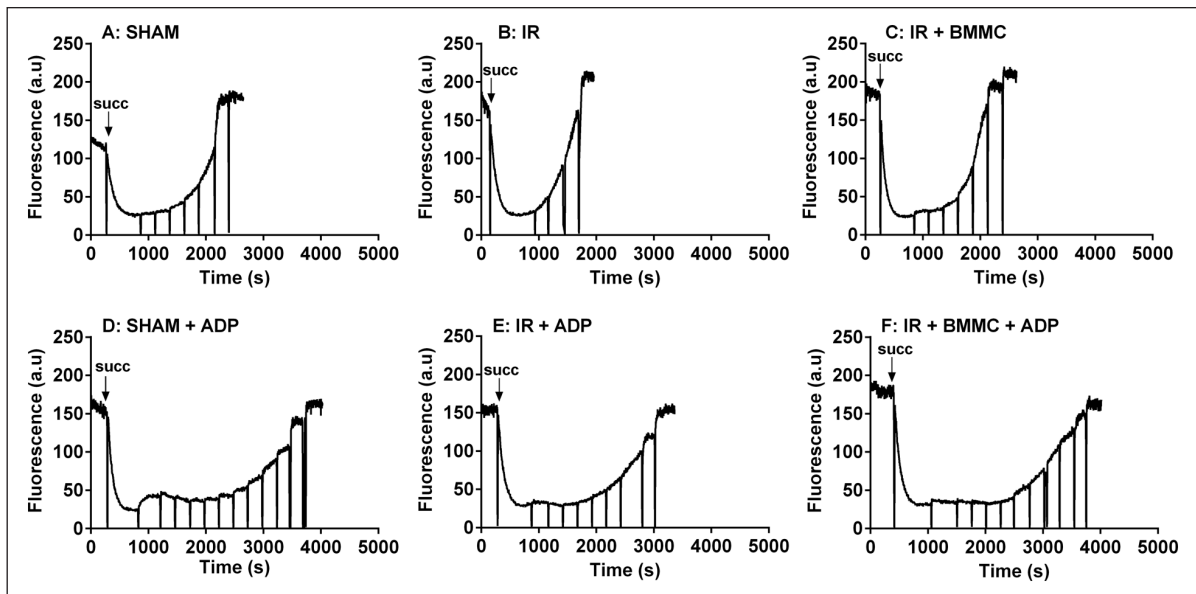
Figure 4. Accelerated Ca^{2+}-induced depolarization of inner mitochondrial membrane after IR. Representative recordings of Safranin O fluorescence after energization of mitochondria by addition of 10 mM succinate (arrows) in the absence (A–C) or presence of 1 mM ADP (D–F). Mitochondria (0.1 mg/ml) from SHAM (A, D), IR (B, E), or IR + BMMC (C, F) were incubated in Safranin O-containing medium (see "Materials and Methods" section) supplied with successive additions of CaCl$_2$ pulses (10 µM) at the times indicated on the *abscissae* (after the first arrow). In the experiments performed in the presence of ADP, it was supplied before the first addition of Ca^{2+}. IR: ischemia followed by reperfusion; BMMC: bone marrow mononuclear cells.

demonstrated[19]. The following experiments investigated whether replenishing of the Krebs cycle with 2C fragments[25] is affected by IR and recovered by BMMC, as described for Ca^{2+} transport and Ca^{2+}-induced modifications of mitochondrial membrane potential. Initially, activity was measured to investigate early effects at 1 h of reperfusion (Fig. 7A), as in the case of the other two processes above. Unexpectedly, the activity was similar in SHAM and IR groups, and 70% higher in IR + BMMC. We further investigated this result in experiments with a 24-h longer period of reperfusion (Fig. 7B), that showed the recovery of citrate synthase activity in SHAM and IR mitochondria to the levels in the group IR + BMMC, which remained similar to that seen after 1 h of reperfusion. This scenario is better seen in Fig. 8, which compares the activity in the three groups at two times: spontaneous and significant increase in SHAM and IR mitochondria with time, without modification in the case of IR + BMMC.

Discussion

The main findings of this study were that BMMC recover the Ca^{2+} handling in renal cortical mitochondria isolated after IR, and that it ameliorated the response of mitochondrial membrane potential to depolarizing Ca^{2+} pulses. The immediate paracrine effects of BMMC, which result in important improvements in renal function[20–22], seem to rely

on the preservation of the finely regulated mechanisms of Ca^{2+} handling, as demonstrated here. In previous studies, we have demonstrated that IR impairs mitochondrial respiration in both basal and phosphorylating conditions, as well as the generation of mitochondrial membrane potential[19]. The present data indicate that altered mechanisms for uptake and release of Ca^{2+} are key in processes that culminate in reduced ATP synthesis in IR. Ca^{2+} is an activator of dehydrogenases[29,30] and therefore of electron fluxes, generation of mitochondrial membrane potential, and ATP synthesis. Deregulation of Ca^{2+} transport mechanisms by IR in a tissular microenvironment with elevated formation of ROS[13,31] could facilitate the opening of PTP, as suggested by the experiments shown in Figs. 2 and 3.

These figures provide evidence that IR induced PTP opening, as suggested by the initially slow and then sudden tendency of a Ca^{2+} efflux (the smooth curve in Fig. 3A). We propose that PTP opening is prevented by BMMC because the effect is similar to that encountered in the presence of CsA, which reverses the IR-induced alterations in mitochondrial Ca^{2+} handling. Decrease in the extra-mitochondrial [Ca^{2+}] after successive Ca^{2+} pulses (decrease in the first-order constant of the departure from the baseline of Calcium green fluorescence from 0.0051 to 0.0039 µM^{-1} min^{-1}; see Fig. 2H), the recovery of the net rate of Ca^{2+} influx, and the demonstration that extra [Ca^{2+}] (more 60%) that can be provided to the medium before the beginning of the Ca^{2+} efflux tendency in the presence of CsA (shaded area
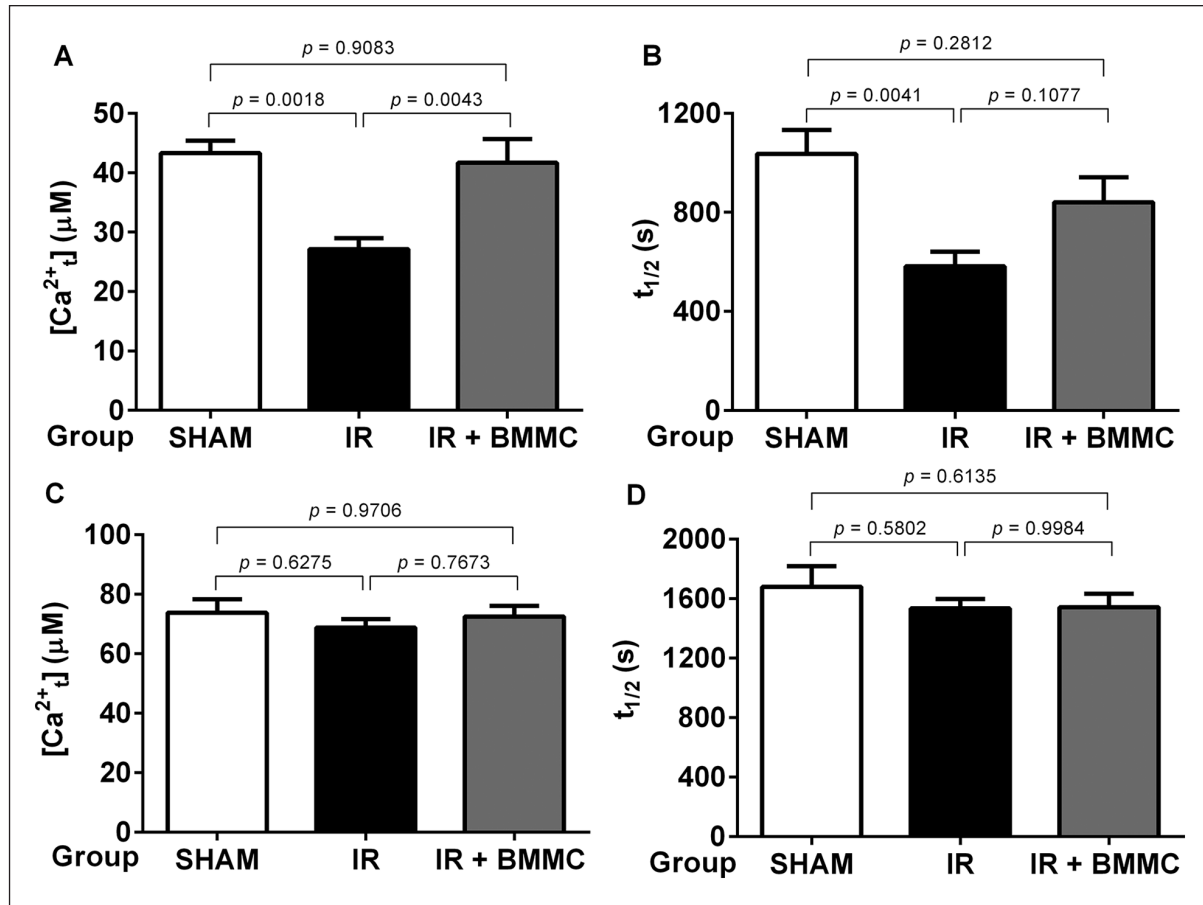
Figure 5. Ca^{2+}-induced depolarization of the mitochondrial internal membrane. Ca^{2+} load required for total depolarization ($[Ca^{2+}]t$) (A, C) and time required for half-depolarization ($t_{1/2}$) (B, D). Assay conditions were as described in the legend to Fig. 4 and in the "Materials and Methods" section, in the absence (A, B) or presence of 1 mM ADP (C, D). Bars represent means ± SEM. Groups are indicated on the *abscissae*. Using one-way ANOVA followed by Tukey's test assessed differences, which are indicated within the panels. Without ADP: SHAM, $n = 6$; IR, $n = 8$; IR + BMMC, $n = 6$. With ADP: SHAM, $n = 9$; IR, $n = 9$; IR + BMMC, $n = 9$. SEM: standard error of the mean; ANOVA: analysis of variance; IR: ischemia followed by reperfusion; BMMC: bone marrow mononuclear cells.
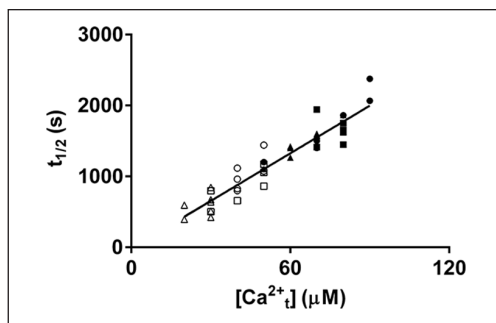

Figure 6. Linear correlation between $[Ca^{2+}]t$ and the corresponding $t_{1/2}$ of depolarization. Values are those taken from Fig. 5. Empty symbols: assays in the absence of ADP. Filled symbols: assays in the presence of 1 mM ADP. SHAM: empty and filled circles. IR: empty and filled triangles. IR + BMMC: empty and filled squares. The linear function $t_{1/2} = 22.1\ \mu M^{-1}s \times [Ca^{2+}]t$ was adjusted to the experimental values by least squares ($P < 0.0001$). IR: ischemia followed by reperfusion; BMMC: bone marrow mononuclear cells.

in Fig. 3B) give support to this view. CsA inhibits PTP opening[32] and reduces cell death[33,34], which is a prominent event in renal IR[19] mediated by PTP opening, as also demonstrated in heart lesions[13,35,36].

The target for the alterations by IR of the renal mitochondrial Ca^{2+} influx is possibly the mitochondrial Ca^{2+} uniporter (MCU)[37,38], its tetrameric structure preserved from fungi to humans[39,40] being destabilized by the intense production of ROS after IR. In a recent communication[41], we demonstrated that intense oxidative stress is responsible for the early lesions caused by IR, which is avoided by administration of the main paracrine secretion of stem and mesenchymal cells (MSC)—the EVs they secrete[42]. BMMC, which contains a small parcel of MSC[43], has the same effect in preserving renal structures[14,15,17,22,44], demonstrating that they contain a population of cells that helps in the preservation of renal structure and function. Moreover, BMMC also secretes EVs, and blockade of EV secretion by GW4869 cancels the repair of an infarcted myocardium, as was recently demonstrated[45].
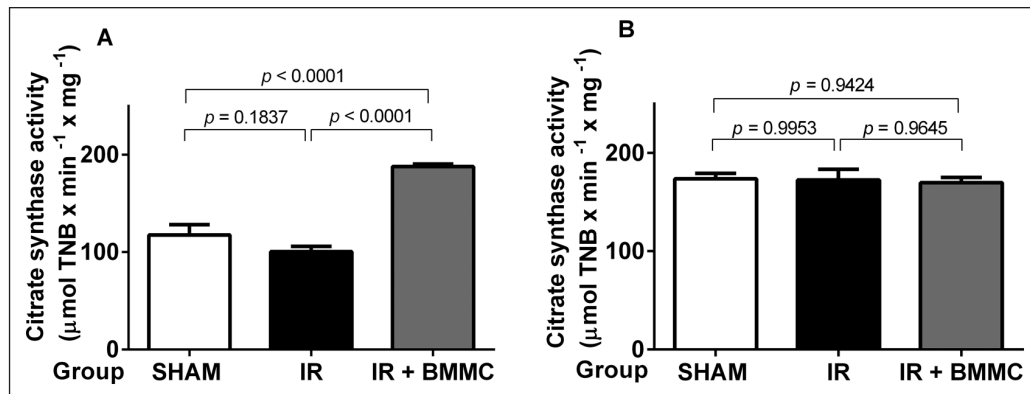
Figure 7. BMMC stimulate citrate synthase activity. Citrate synthase activity was measured 1 h (A) and 24 h (B) after IR, as described in the "Materials and Methods" section. Groups are indicated on the *abscissae*. Bars represent means ± SEM. Differences were assessed with the use of one-way ANOVA followed by Tukey's test, which are indicated within the panels. After 1 h: SHAM, $n = 6$; IR, $n = 6$; IR + BMMC, $n = 9$. After 24 h: SHAM, $n = 5$; IR, $n = 7$; IR + BMMC, $n = 9$. BMMC: bone marrow mononuclear cells; IR: ischemia followed by reperfusion; SEM: standard error of the mean; ANOVA: analysis of variance; TNB: 5-thio-2-nitrobenzoic acid.
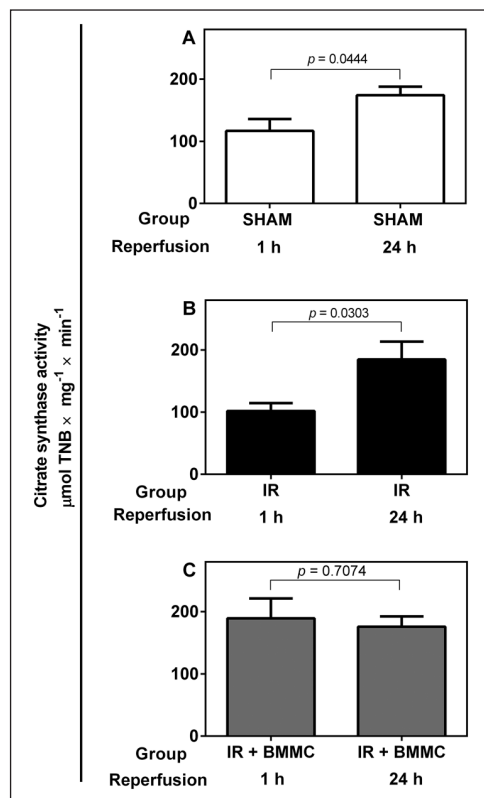
Figure 8. Evolution of citrate synthase activity between 1 and 24 h of interventions: (A) SHAM, (B) IR, and (C) IR + BMMC. Data and times are those described in the legend to Fig. 7 for the different groups and treatments. Bars represent means ± SEM. Differences between 1 and 24 h were assessed with the use of unpaired Student's *t* test within each experimental group; the *P* values are indicated within the panels. IR: ischemia followed by reperfusion; BMMC: bone marrow mononuclear cells; SEM: standard error of the mean; TNB: 5-thio-2-nitrobenzoic acid.

As inhibition of catalase suppresses the beneficial effects of EVs[46], it is plausible that the effects of BMMC seen in Fig. 3 rely on the restoration of the normal redox environment, which is highly altered after IR in the kidney and heart[13,22,47–49]. In the kidney, intravenous injection of BMMC is cytoprotective and has regenerative properties in a rat model of IR by modulating oxidative and inflammatory processes[22].

CsA-sensitive PTP also modulates physiologically the mitochondrial membrane potential and local Ca^{2+} signals in mitochondria[50]. However, long-lasting, deregulated PTP opening, together with exacerbated oxidative stress, is associated with several pathological processes in mitochondria, including the collapse of the mitochondrial membrane potential[51,52]. It is plausible to associate the accelerated collapse of $\Delta\Psi$ to alterations in IR-induced Ca^{2+} handling for two reasons. First, IR decreased the tightly associated (Fig. 6) $[Ca^{2+}]_t$ and the $t_{1/2}$ required for Ca^{2+}-induced depolarization (Figs. 4 and 5A, B). Second, the influence of IR was not detected in both parameters in the presence of ADP (Fig. 5C, D), probably because the nucleotide decreases the opening of PTP[53] through a mechanism that seems to involve an increase in the K_m of Ca^{2+}-induced PTP opening, as proposed by Bauer and Murphy[13]. Stabilization of adenine nucleotide translocase (ANT) by ADP in a conformation facing the matrix inhibits PTP opening[35], which could explain why the influence of IR in $[Ca^{2+}]_t$ and $t_{1/2}$ is not seen when ADP is present in the assays.

The influence of ADP on the Ca^{2+}-induced depolarization in IR opens up the possibility of an additional target for the injury and for the beneficial effect of BMMC administration, namely, the transport of Ca^{2+} across the outer mitochondrial membrane (OMM). Ca^{2+} uptake across the OMM is mediated and regulated by voltage-dependent anion channels (VDACs) that form large Ca^{2+} pores[54,55], which are modulated by

interactions between the channel and ANT. Allouche et al[56] demonstrated the existence of a direct VDAC-ANT interaction and, several years before[57,58] (cf. Bauer and Murphy[13]), it was proposed that they form a complex in physiological and pathological conditions (including IR). Thus, this complex could participate in PTP opening as a consequence of IR, making it possible that BMMC secrete factors (including EV) that restore the architecture and function of the VDAC-ANT complex together with those of MCU.

The generation of the mitochondrial membrane potential and its utilization to synthesize ATP by the F_oF_1-ATP synthase requires an appropriate seeding of the Krebs cycle and the mitochondrial electron transport. The citrate synthase is the key enzyme at the beginning of the cycle that ensures the continuous supply of 2 C atoms[25], and for this reason we investigated whether it was affected by IR and recovered or preserved by BMMC. One hour after the recovery of reperfusion (1.5 h after the beginning of the surgery), the SHAM and IR levels (Fig. 7A) were similar and, possibly, this was a consequence of the renal pedicle manipulation, without any additional influence of arterial clamping and PTP opening. Possibly because the impact on the enzyme was mild and independent of mitochondrial Ca^{2+} disturbance, activity in the SHAM and IR rats increased in the following 24 h, reaching the levels encountered in the group IR + BMMC 1 h after the acute lesion (Fig. 7B). Thus, it may be that the IR + BMMC levels are the "true" normal values, preserved by BMMC administration. Manipulation of the renal pedicle in SHAM mice provokes a specific transcriptional response of vimentin, a marker of renal lesion[59], which involves the sympathetic nervous system and the local renin–angiotensin system that are also crucial for the pathogenesis of renal lesions in IR[60].

In conclusion, we have demonstrated that BMMC prevent renal mitochondrial lesions during the AKI caused by IR through mechanisms associated with the preservation of Ca^{2+} influx and release, and with the response of $\Delta\Psi$ to Ca^{2+}. It is possible that the preservation of these mechanisms relies—at least in part—on the control of the microenvironmental production of ROS[41] in early periods after IR.

Ethical Approval

All experimental protocols followed the guidelines of the Committee of Ethics in the Use of Animals for Research at Federal University of Rio de Janeiro, Brazil (approval number: 104).

Statement of Human and Animal Rights

This article does not contain any studies with human or animal subjects.

Statement of Informed Consent

There are no human subjects in this article, and informed consent is not applicable.

Declaration of Conflicting Interests

The author(s) declared no potential conflicts of interest with respect to the research, authorship, and/or publication of this article.

ORCID iD

Adalberto Vieyra https://orcid.org/0000-0002-8009-7273

References

1. Thadhani R, Pascual M, Bonventre JV. Acute renal failure. N Engl J Med. 1996;334:1448–60.
2. Doi K, Noiri E. Mitochondrial dysfunction in cardiorenal syndrome. Antioxid Redox Signal. 2016;25:200–207.
3. Singbartl K, Kellum JA. AKI in the ICU: definition, epidemiology, risk stratification, and outcomes. Kidney Int. 2012;81:819–25.
4. International Society of Nephrology. Acute kidney injury; 2021. [Accessed August 12, 2021]. https://www.theisn.org/commitment-to-kidney-health/focus-areas/acute-kidney-injury/.
5. Hsu RK, Hsu CY. The role of acute kidney injury in chronic kidney disease. Semin Nephrol. 2016;36:283–92.
6. Hsu CY, Ordoñez JD, Chertow GM, Fan D, McCulloch CE, Go AS. The risk of acute renal failure in patients with chronic kidney disease. Kidney Int. 2008;74:101–107.
7. Giraud S, Favreau F, Chatauret N, Thuillier R, Maiga S, Hauet T. Contribution of large pig for renal ischemia-reperfusion and transplantation studies: the preclinical model. J Biomed Biotechnol. 2011;2011:532127.
8. Basile DP, Anderson MD, Sutton TA. Pathophysiology of acute kidney injury. Compr Physiol. 2012;2:1303–53.
9. Chouchani ET, Pell VR, Gaude E, Aksentijević D, Sundier SY, Robb EL, Logan A, Nadtochiy SM, Ord ENJ, Smith AC, Eyassu F, et al. Ischaemic accumulation of succinate controls reperfusion injury through mitochondrial ROS. Nature. 2014;515:431–35.
10. Chouchani ET, Pell VR, James AM, Work LM, Saeb-Parsy K, Frezza C, Krieg T, Murphy MP. A unifying mechanism for mitochondrial superoxide production during ischemia-reperfusion injury. Cell Metab. 2016;23:254–63.
11. Martin JL, Gruszczyk AV, Beach TE, Murphy MP, Saeb-Parsy K. Mitochondrial mechanisms and therapeutics in ischaemia reperfusion injury. Pediatr Nephrol. 2019;34:1167–74.

12. Ratliff BB, Abdulmahdi W, Pawar R, Wolin MS. Oxidant mechanisms in renal injury and disease. Antioxid Redox Signal. 2016;25:119–46.

13. Bauer TM, Murphy E. Role of mitochondrial calcium and the permeability transition pore in regulating cell death. Circ Res. 2020;126:280–93.

14. Poulsom R, Forbes SJ, Hodivala-Dilke K, Ryan E, Wyles S, Navaratnarasah S, Jeffery R, Hunt T, Alison M, Cook T, Pusey C, et al. Bone marrow contributes to renal parenchymal turnover and regeneration. J Pathol. 2001;195:229–35.

15. Kale S, Karihaloo A, Clark PR, Kashgarian M, Krause DS, Cantley LG. Bone marrow stem cells contribute to repair of the ischemically injured renal tubule. J Clin Invest. 2003;112:42–49.

16. Humes HD, Szczypka MS. Advances in cell therapy for renal failure. Transpl Immunol. 2004;12:219–27.

17. Huls M, Russel FG, Masereeuw R. Insights into the role of bone marrow-derived stem cells in renal repair. Kidney Blood Press Res. 2008;31:104–10.

18. Erpicum P, Weekers L, Detry O, Bonvoisin C, Delbouille MH, Grégoire C, Baudoux E, Briquet A, Lechanteur C, Maggipinto G, Somja J, et al. Infusion of third-party mesenchymal stromal cells after kidney transplantation: a phase I-II, open-label, clinical study. Kidney Int. 2019;95:693–707.

19. Beiral HJ, Rodrigues-Ferreira C, Fernandes AM, Gonsalez SR, Mortari NC, Takiya CM, Sorenson MM, Figueiredo-Freitas C, Galina A, Vieyra A. The impact of stem cells on electron fluxes, proton translocation, and ATP synthesis in kidney mitochondria after ischemia/reperfusion. Cell Transplant. 2014;23:207–20.

20. Zubko R, Frishman W. Stem cell therapy for the kidney? Am J Ther. 2009;16:247–56.

21. Yuen DA, Gilbert RE, Marsden PA. Bone marrow cell therapies for endothelial repair and their relevance to kidney disease. Semin Nephrol. 2012;32:215–23.

22. Ornellas FM, Ornellas DS, Martini SV, Castiglione RC, Ventura GM, Rocco PR, Gutfilen B, de Souza SA, Takiya CM, Morales MM. Bone marrow-derived mononuclear cell therapy accelerates renal ischemia-reperfusion injury recovery by modulating inflammatory, antioxidant and apoptotic related molecules. Cell Physiol Biochem. 2017;41:1736–52.

23. Kolonics F, Szeifert V, Timár CI, Ligeti E, Lőrincz ÁM. The functional heterogeneity of neutrophil-derived extracellular vesicles reflects the status of the parent cell. Cells. 2020;9:2718.

24. Kolonics F, Kajdácsi E, Farkas VJ, Veres DS, Khamari D, Kittel Á, Merchant ML, McLeish KR, Lőrincz ÁM, Ligeti E. Neutrophils produce proinflammatory or anti-inflammatory extracellular vesicles depending on the environmental conditions. J Leukoc Biol. 2021;109:793–806.

25. Wiegand G, Remington SJ. Citrate synthase: structure, control, and mechanism. Annu Rev Biophys Biophys Chem. 1986;15:97–117.

26. Rossaint J, Kühne K, Skupski J, Van Aken H, Looney MR, Hidalgo A, Zarbock A. Directed transport of neutrophil-derived extracellular vesicles enables platelet-mediated innate immune response. Nat Commun. 2016;7:13464.

27. Whittembury G, Proverbio F. Two modes of Na extrusion in cells from guinea pig kidney cortex slices. Pflugers Arch. 1970;316:1–25.

28. Lowry OH, Rosebrough NJ, Farr AL, Randall RJ. Protein measurement with the Folin phenol reagent. J Biol Chem. 1951;193:265–75.

29. Denton RM, McCormack JG. The role of calcium in the regulation of mitochondrial metabolism. Biochem Soc Trans. 1980;8:266–68.

30. Diaz-Juarez J, Suarez JA, Dillmann WH, Suarez J. Mitochondrial calcium handling and heart disease in diabetes mellitus. Biochim Biophys Acta Mol Basis Dis. 2021;1867:165984.

31. Collino F, Lopes JA, Corrêa S, Abdelhay E, Takiya CM, Wendt CHC, de Miranda KR, Vieyra A, Lindoso RS. Adipose-derived mesenchymal stromal cells under hypoxia: changes in extracellular vesicles secretion and improvement of renal recovery after ischemic injury. Cell Physiol Biochem. 2019;52:1463–83.

32. Crompton M, Ellinger H, Costi A. Inhibition by cyclosporin A of a Ca2+-dependent pore in heart mitochondria activated by inorganic phosphate and oxidative stress. Biochem J. 1988;255:357–60.

33. Nazareth W, Yafei N, Crompton M. Inhibition of anoxia-induced injury in heart myocytes by cyclosporin A. J Mol Cell Cardiol. 1991;23:1351–54.

34. Carroll J, He J, Ding S, Fearnley IM, Walker JE. Persistence of the permeability transition pore in human mitochondria devoid of an assembled ATP synthase. Proc Natl Acad Sci U S A. 2019;116:12816–21.

35. Halestrap AP, Pasdois P. The role of the mitochondrial permeability transition pore in heart disease. Biochim Biophys Acta. 2009;1787:1402–415.

36. Assaly R, de Tassigny A, Paradis S, Jacquin S, Berdeaux A, Morin D. Oxidative stress, mitochondrial permeability transition pore opening and cell death during hypoxia-reoxygenation in adult cardiomyocytes. Eur J Pharmacol. 2012;675:6–14.

37. De Stefani D, Raffaello A, Teardo E, Szabò I, Rizzuto R. A forty-kilodalton protein of the inner membrane is the mitochondrial calcium uniporter. Nature. 2011;476:336–40.

38. Baughman JM, Perocchi F, Girgis HS, Plovanich M, Belcher-Timme CA, Sancak Y, Bao XR, Strittmatter L, Goldberger O, Bogorad RL, Koteliansky V, et al. Integrative genomics identifies MCU as an essential component of the mitochondrial calcium uniporter. Nature. 2011;476:341–45.

39. Baradaran R, Wang C, Siliciano AF, Long SB. Cryo-EM structures of fungal and metazoan mitochondrial calcium uniporters. Nature. 2018;559:580–84.

40. Wang Y, Nguyen NX, She J, Zeng W, Yang Y, Bai XC, Jiang Y. Structural mechanism of EMRE-dependent gating of the human mitochondrial calcium uniporter. Cell. 2019;177:1252–61.

41. Vieyra A, Lopes JA, Collino F, Sampaio LS, Costa-Sarmento G, Wendt CHC, Almeida FP, Miranda KR, Kasai-Brunswick TH, Lindoso RS. Early effects of extracellular vesicles secreted by adipose tissue mesenchymal cells in renal ischemia followed by reperfusion: mechanisms rely in the restoration of the redox tissular environment. Abstract 11th meeting of the Brazilian Association of Cell and Gene Therapy and 1st International Society of Cell Therapy South and Central America Regional Forum, Curitiba, Brazil. Cytotherapy. 2021;23(Suppl):11.

42. Maacha S, Sidahmed H, Jacob S, Gentilcore G, Calzone R, Grivel JC, Cugno C. Paracrine mechanisms of mesenchymal stromal cells in angiogenesis. Stem Cells Int. 2020; 2020:4356359.

43. Fox JM, Chamberlain G, Ashton BA, Middleton J. Recent advances into the understanding of mesenchymal stem cell trafficking. Br J Haematol. 2007;137:491–502.

44. Barreira AL, Takiya CM, Castiglione RC, Maron-Gutierrez T, Barbosa CM, Ornellas DS, Verdoorn KS, Pascarelli BM, Borojevic R, Einicker-Lamas M, Leite M Jr, et al. Bone marrow mononuclear cells attenuate interstitial fibrosis and stimulate the repair of tubular epithelial cells after unilateral ureteral obstruction. Cell Physiol Biochem. 2009;24:585–94.

45. Yeganeh A, Alibhai FJ, Tobin SW, Lim F, Wu J, Li S, Weisel RD, Li RK. Age-related defects in autophagy alter the secretion of paracrine factors from bone marrow mononuclear cells. Aging (Albany NY). 2021;13:14687–708.

46. de Godoy MA, Saraiva LM, de Carvalho LRP, Vasconcelos-Dos-Santos A, Beiral HJV, Ramos AB, Silva LRP, Leal RB, Monteiro VHS, Braga CV, de Araujo-Silva CA, et al. Mesenchymal stem cells and cell-derived extracellular vesicles protect hippocampal neurons from oxidative stress and synapse damage induced by amyloid-β oligomers. J Biol Chem. 2018;293:1957–75.

47. Sung FL, Zhu TY, Au-Yeung KK, Siow YL, O K. Enhanced MCP-1 expression during ischemia/reperfusion injury is mediated by oxidative stress and NF-kappaB. Kidney Int. 2002;62:1160–70.

48. Kaminski KA, Bonda TA, Korecki J, Musial WJ. Oxidative stress and neutrophil activation–the two keystones of ischemia/reperfusion injury. Int J Cardiol. 2002;86:41–59.

49. Caio-Silva W, da Silva Dias D, Junho CVC, Panico K, Neres-Santos RS, Pelegrino MT, Pieretti JC, Seabra AB, De Angelis K, Carneiro-Ramos MS. Characterization of the oxidative stress in renal ischemia/reperfusion-induced cardiorenal syndrome type 3. Biomed Res Int. 2020;2020:1605358.

50. Smaili SS, Russell JT. Permeability transition pore regulates both mitochondrial membrane potential and agonist-evoked Ca2+ signals in oligodendrocyte progenitors. Cell Calcium. 1999;26:121–30.

51. Bernardi P, Rasola A, Forte M, Lippe G. The mitochondrial permeability transition pore: channel formation by F-ATP synthase, integration in signal transduction, and role in pathophysiology. Physiol Rev. 2015;95:1111–55.

52. Šileikytė J, Forte M. The mitochondrial permeability transition in mitochondrial disorders. Oxid Med Cell Longev. 2019;2019:3403075.

53. Gizatullina ZZ, Chen Y, Zierz S, Gellerich FN. Effects of extramitochondrial ADP on permeability transition of mouse liver mitochondria. Biochim Biophys Acta. 2005;1706:98–104.

54. Sander P, Gudermann T, Schredelseker J. A calcium guard in the outer membrane: is VDAC a regulated gatekeeper of mitochondrial calcium uptake? Int J Mol Sci. 2021;22:946.

55. Hoogerheide DP, Rostovtseva TK, Bezrukov SM. Exploring lipid-dependent conformations of membrane-bound α-synuclein with the VDAC nanopore. Biochim Biophys Acta Biomembr. 2021;1863:183643.

56. Allouche M, Pertuiset C, Robert JL, Martel C, Veneziano R, Henry C, dein OS, Saint N, Brenner C, Chopineau J. ANT-VDAC1 interaction is direct and depends on ANT isoform conformation in vitro. Biochem Biophys Res Commun. 2012;429:12–17.

57. Henderson PJ, Lardy HA. Bongkrekic acid. An inhibitor of the adenine nucleotide translocase of mitochondria. J Biol Chem. 1970;245:1319–26.

58. Novgorodov SA, Gudz TI, Jung DW, Brierley GP. The nonspecific inner membrane pore of liver mitochondria: modulation of cyclosporin sensitivity by ADP at carboxyatractyloside-sensitive and insensitive sites. Biochem Biophys Res Commun. 1991;180:33–38.

59. Vansthertem D, Gossiaux A, Declèves AE, Caron N, Nonclercq D, Legrand A, Toubeau G. Expression of nestin, vimentin, and NCAM by renal interstitial cells after ischemic tubular injury. J Biomed Biotechnol. 2010;2010:193259.

60. Panico K, Abrahão MV, Trentin-Sonoda M, Muzi-Filho H, Vieyra A, Carneiro-Ramos MS. Cardiac inflammation after ischemia-reperfusion of the kidney: role of the sympathetic nervous system and the renin-angiotensin system. Cell Physiol Biochem. 2019;53:587–605.